Space Charge Measurement by Electroacoustic Method: Impact of Acoustic Properties of Materials on The Response for Different Geometries

Thi Thu Nga Vu, Laurent Berquez, Gilbert Teyssedre

Space charge measurement by electroacoustic method: impact of acoustic properties of materials on the response for different geometries

T.T.N. Vu

Electric Power University,
Hanoi, Vietnam
L. Berquez, G. Teyssèdre

Laplace, University of Toulouse, CNRS, UPS, INPT,
Toulouse, France.

Abstract: The pulsed electro-acoustic method (PEA) allows dynamic measurements of space charge density distribution with good temporal resolution and is suitable for both flat samples (a few hundred micrometers thickness) and coaxial cable samples. The response obtained by the technique is tributary to the electro-mechanical properties of the materials through which acoustic waves propagate. Hence, when dealing with multilayer dielectrics, the acoustic properties of individual layers are to be taken into account. Also, the acoustic attenuation and dispersion phenomena, especially when dealing with relatively thick samples, affect the space charge resolution at positions far away from the sensor. Therefore, application of a calibration procedure on experimental signals is necessary to recover space charge density profile from PEA raw signals and to provide real results on charge density both on its temporal and spatial dependence. We illustrate here in different samples configurations, spanning from flat samples, multi-layer and cable geometry, how the calibration is achieved and how the acoustic properties of materials impart the response.

Keywords: Pulse electroacoustic method, deconvolution, acoustic properties, dielectrics, space charges

1. Introduction

The need for knowledge about space charge formation and accumulation mechanisms in insulating materials led to the development in past decades of new measurement techniques giving access to spatial distribution of charge density - and thus of electric field. The low mobility of carriers in polymeric insulators allows non-destructive spatially resolved measurement of charge density. These non-destructive techniques, with spatial resolution, include three families according to the nature of perturbation introduced to probe charges [1, 2]: methods based on thermal perturbation of various shape (Thermal Pulse, Light Intensity Modulation Method, Thermal Step), acoustic wave (Piezoelectrically Induced Pressure Wave, Laser Induced Pressure Pulse) and electric field pulse in pulsed electro-acoustic method (PEA). These three groups of non-destructive techniques are based on the same principle in which a non-homogeneous perturbation of the electrostatic state (elastic forces in case of PEA) is introduced by an external stimulus [3].

In the group of thermal methods, diffusion of heat is used to modify the equilibrium of charges through permittivity variation and volume expansion and thus induce an electrical response. Acoustic methods use deformation produced by propagation of pressure waves to modify the electrostatic equilibrium and to induce an electrical signal. Finally, the electro-acoustic method relies on an excitation by electric field pulses; the electrostatic force produced by interaction with the charges generates a mechanical response. Various techniques currently make it possible to establish charge density distribution in polymer insulators; however, depending on the technique used, each type of measurement technique has advantages and drawbacks.

The PEA method was developed in 1985 by Japanese researchers (T. Maeno, T. Takada and their collaborators [4], [5]). The method consists of applying electric field pulses (of the order of 1 kV/mm) of very short duration (of the order of one nanosecond) through a sample. The production of a Coulomb type force induces a transient elementary displacement of the charge cloud around its equilibrium position. Then, two acoustic waves, of amplitude proportional to the quantity of charges, are generated. One is in extension; the other in compression and they propagate in opposite directions. One of these pressure waves is detected by means of a piezoelectric sensor (lower electrode) which converts the acoustic signal into an electrical signal. The electrical signal is amplified before being recorded using a digital oscilloscope. Adequate signal processing then makes it possible to recover the space charge density profile.

The PEA method has the advantage of being able to perform measurements in the presence of external voltage (DC or AC). It is therefore perfectly suited to study the mechanisms of injection and transport of charges in the insulation of high voltage cables [6].

In the case of conventional PEA method, for flat specimen, the sample is placed between two electrodes (Figure 1). The upper electrode is made of a semiconducting material, i.e. a polymer doped with carbon black particles having acoustic properties approaching those of the polymeric sample such as to minimize wave reflections at the interface with the sample. This electrode is connected to the high voltage power supply and the pulse generator. The lower aluminium electrode is connected to ground. A piezoelectric sensor, usually Poly (Vinylidene Fluoride) – PVDF, with some attempts of using Lithium Niobate material with higher thermal withstanding [7], is placed under the lower electrode and converts the acoustic wave into an electrical signal. Finally, under the piezoelectric sensor is placed an acoustic absorber usually made of poly(methyl methacrylate) – PMMA intended to produce only a positive reflection, which allows to remove a pole in the sensor response.

The principle of the PEA technique for cables (coaxial geometry) is similar to that of the conventional PEA method. However, the space charge recovery technique for PEA cable needs to take into account cylindrical geometry, along with the attenuation and the dispersion of the acoustic waves when the insulation is relatively thick.

2. Sensor response

According to the scheme given in Figure 1, acoustic waves generated by a sheet of charges propagate in opposite directions, one of them being directed towards the piezoelectric sensor. We designate by $p_{Al}(t)$ the pressure wave reaching the interface between the Al ground electrode and the piezoelectric sensor. We consider first how the acoustic waves are converted into an electrical signal.

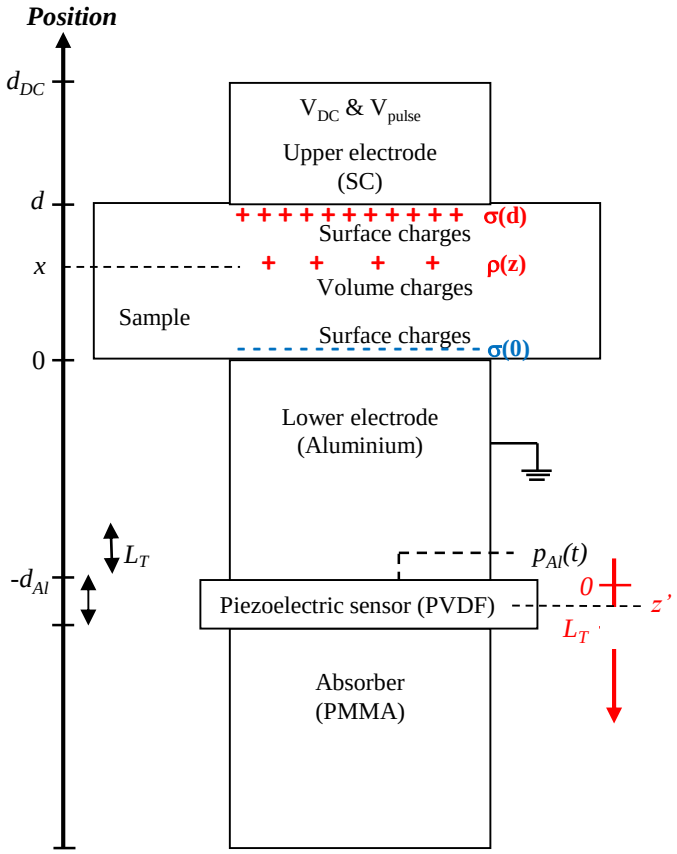

Figure 1: Principle and main elements of a PEA test cell

A. Piezoelectric sensor response

When entering in the PVDF, the acoustic wave generates at point z' (z'=-x + d_{Al} , cf. Figure 1) a polarization $P_P(z')$ proportional to the mechanical stress. Therefore, the voltage at PVDF bounds in open circuit conditions is given by [8]:

$$V_i(t) = \int_0^{L_T} -E(z',t)dz' = \int_0^{L_T} \frac{1}{\varepsilon_{Piezo}} P_P(z',t)dz' = g_{33}\int_0^{L_T} p_{Piezo}(z',t)dz' \qquad (1)$$

where g_{33} is the piezoelectric coefficient, ε_{Piezo} the sensor dielectric permittivity and L_T its thickness.

The pressure inside the sensor is related to that at its entrance by:

$$p_{Piezo}(z', t) = T_{Al-PVDF} \cdot p_{Al}\left(t - \frac{z'}{v_{Piezo}}\right) \quad (2)$$

where $T_{Al\text{-}PVDF}$ is the transmission coefficient of acoustic wave at Al/PVDF interface and v_{Piezo} is the sound velocity. Writing:

$$\tau' = \frac{z'}{v_{Piezo}} \quad (3)$$

we obtain:

$$V_i(t) = \frac{g_{33} \cdot T_{Al-PVDF}}{v_{Piezo}} \int_0^{L_T/v_{Piezo}} p_{Al}(t - \tau) d\tau' \quad (4)$$

This can be written as the convolution between the transfer function of the piezoelectric sensor h(t) and pressure entering in the sensor $p_{Al}(t)$. If the response of the piezoelectric sensor is homogeneous along its thickness, h(t) can be considered as a rectangular window function Π: $V_i(t)$ is given, with a coefficient, by a convolution equation:

$$V_i(t) = \frac{g_{33} \cdot T_{Al-PVDF}}{v_{Piezo}} \int_{-\infty}^{+\infty} \prod\left(\frac{t}{L_T/v_{Piezo}} - 1/2\right) p_{Al}(t - \tau) d\tau' \propto h(t) * p_{Al}(t) \quad (5)$$

with

$$h(t) = \prod\left(\frac{t}{L_T/v_{Piezo}} - 1/2\right) \quad (6)$$

Expression (5) allows qualitative analysis of the effect of the piezoelectric sensor thickness on signal $V_i(t)$. To simplify our analysis, the pulse is assumed of a rectangular type.

B. Transducer response (Piezoelectric sensor + Amplifier)

One face of the piezo sensor is connected to a broadband amplifier having an input impedance R_E of 50Ω. The transducer can be modelled by the RC circuit of Figure 2 [8].

The impulse response of the circuit (high-pass) is given by:

$$g(t) = \delta(t) - \frac{1}{\tau_e} \exp\left(\frac{-t}{\tau_e}\right) . u(t) \quad (7)$$

where $\tau_e = R_E.C_0$, C_0 is the effective capacity of the transducer. u(t) is a step function. Therefore, the response $V_S(t)$ at the output of the amplifier is:

$$V_s(t) = g(t) * V_i(t) \quad (8)$$

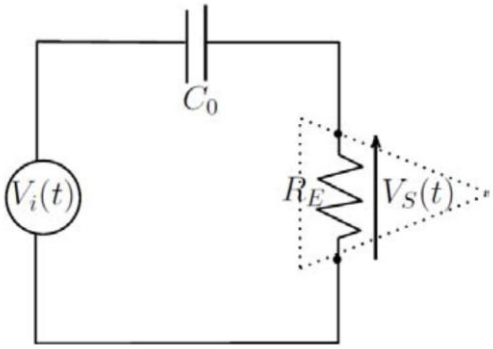

Figure 2: Transducer equivalent circuit [8]

The transducer produces a voltage by integrating stress across its thickness (cf. Eq. 5) which is then detected through the high-pass filter [8]. The frequency response of the transducer depends on the transit time $\tau_a = \mathrm{L_T}/\mathrm{v_{Piezo}}$ and the time constant $\tau_e = R_E.C_0$. Depending of these two time constants, the transducer could have different responses. A flat response can be obtained if $\tau_a \gg \tau_e$. In this case the piezoelectric sensor is thicker than the acoustic signal and is connected to a low impedance amplifier. As a result, the output will be proportional to the acoustic signal and the time domain signal will trace the charge distribution. For a piezoelectric sensor sandwiched between a delay line and an absorber, the signal components near τ_a^{-1} are amplified and the lower frequency components are attenuated. Moreover, this resonant configuration introduces a damped oscillation on the signal.

3. PEA method and deconvolution techniques for flat samples

A. Classic PEA device

The experimental setup used for space charge measurements on flat samples is shown in Figure 3.

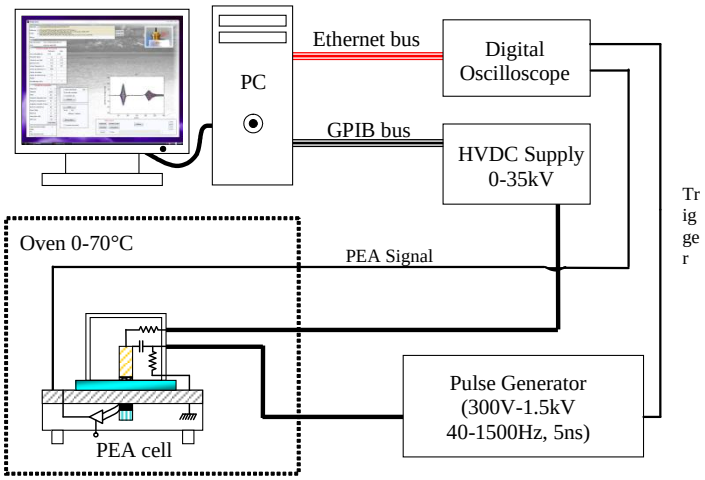

Figure 3: Schematics of the PEA test bench for flat specimen. Adapted from [10].

The PEA cell is placed in an oven allowing measurements under controlled temperature in the range between 0°C and 70°C. This cell, provided by TechImp, Italy, is well suited for measuring space charge in flat samples with thicknesses between 200 and 500 μm. A pulse generator delivers the stimuli necessary for measurement and synchronizes the PEA signals. The maximum amplitude of the pulses is 2 kV and maximum repetition frequency is 50 kHz. The pulses width at half maximum is of the order of 5 ns. The high voltage is supplied by a DC voltage generator provided with polarity reversal module. In addition, the DC high voltage generator can be controlled from a PC via a GPIB bus offering the possibility of programming long-term protocols. A digital storage oscilloscope (DSO) with a 2 GHz bandwidth allows measuring signals from PEA up to 1 GS/s. Thus, very fast signals can be captured with a very acceptable temporal resolution. The DSO exhibits high processing speed offering the possibility of averaging a large number of raw signals in a relatively short time improving the signal-to-noise ratio (SNR). The data is then recorded and processed by means of a computer to recover space charge profiles from deconvolution techniques.

B. Deconvolution technique for flat samples

For a homogeneous insulator, the signal from the piezoelectric sensor in time domain $v_{PEA}(t)$ is given by convolution of the various transfer functions [9], [10]:

$$v_{PEA}(t) = B.\,g(t) * h(t) * r(t) * e\left(t - \frac{d_{Al}}{v_{Al}}\right) \tag{9}$$

where B is a constant; h(t) and g(t) are respectively the transfer function of the transducer and impulse response of sensor defined previously; d_{Al} and v_{Al} are respectively the thickness and velocity of sound in aluminium which constitutes the lower electrode of PEA cell.

The function $r(t) = \rho(t.v_s) = \rho(z)$ represents the space charge density profile along the insulation thickness with v_s the sound velocity in the sample.

The simplest method for charge recovery consists in using spectral division between the measured signal and a calibration signal obtained from a known source of charges, as described below. In the frequency domain, the relationship between signal and charge profile is simplified. Indeed, the Fourier transform of $v_{PEA}(t)$ gives:

$$V_{PEA}(f) = S(f).\,R(f) \tag{10}$$

where S(f) is the transfer function of the whole system

$$S(f) = B.\,G(f).\,H(f).\,E(f).\exp\left(-2i\pi f\frac{d_{Al}}{v_{Al}}\right) \tag{11}$$

This transfer function can be derived from a signal calibration $V_{PEA1}(f)$ produced by capacitive charge (σ_1) formed at lower electrode (connected to ground) when a DC voltage U_{ref} is applied through a sample of thickness d:

$$V_{PEA1}(f) = S(f)\frac{\sigma_1}{v_s} \tag{12}$$

with

$$\sigma_1 = \frac{\varepsilon U_{ref}}{d} \tag{13}$$

We can deduce R(f) :

$$R(f) = \frac{\sigma_1}{v_s}\left[\frac{V_{PEA}(f)}{V_{PEA1}(f)}\right] \tag{14}$$

Moreover, by neglecting the attenuation phenomenon of elastic waves, the space charge profile is given by the real part of inverse Fourier transform of R(f):

$$\rho(t.v_s) = \frac{\sigma_1}{v_s}\mathrm{Re}\left(F^{-1}\left[\frac{V_{PEA}(f)}{V_{PEA1}(f)}\right]\right) \tag{15}$$

The signal processing is performed through Matlab software. The in-built functions are used to calculate direct and inverse Fourier transforms of PEA signals. Since PEA signals have limited frequency bandwidth, the division between the spectrum of signal and that of the reference systematically leads to amplification of high frequency noise. A Gaussian (low-pass) filter is then used after spectral division to eliminate high frequency noise. Note also that the choice of the bandwidth for the Gaussian filter is of great importance with regard to the spatial resolution of charge profile. A synoptic of the signal conditioning for deconvolution method is sketched on Figure 4.

C. Deconvolution technique in the case of bilayer materials

Multilayer specimen can be interesting to investigate, first for fundamental purpose in an attempt to distinguish charges injected at the electrodes from those generated in the volume [11], also to investigate the impact of material modification as with nanocomposites [12]. Space charge was reported in layered films of the same material pointing to specific features at the surface of the film [13, 14]. There are also practical reasons to investigate dielectric stacks with materials of different nature, as with joints in cables [15], or when oil and solid insulations are associated paper-oil insulations [16]. Complex dynamic features are revealed when switching from capacitive to resistive field grading and with interfacial charge development. The case of oil-solid insulation is especially tricky as the time constant for Maxwell interface charge can be relatively short and the acoustic impedance mismatch is relatively high [17].

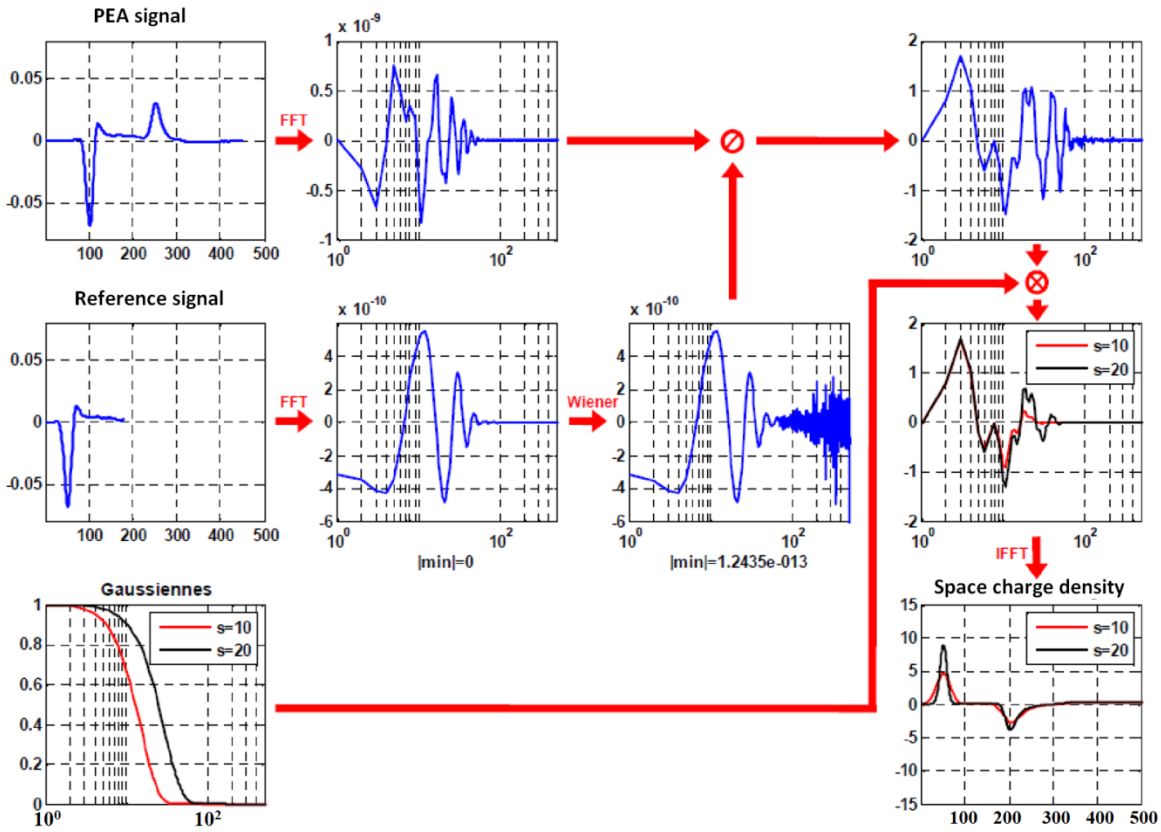

Figure 4: Block diagram of signal processing

We illustrate here the case of association of materials for cable joints, with cross-linked polyethylene – XLPE and rubber material. We assume that the two materials are tightly associated as when crosslinked altogether, layer 1 is rubber – EPDM (ethylene-propylene-diene monomer) and layer 2 is XLPE, cf. Figure 5. For space charge measurement, the voltage is applied on the EPDM as shown in the figure. XLPE is to the ground electrode.

Due to discontinuities on the permittivity and acoustic parameters, in particular the speed of sound, special attention must be paid to the processing of raw PEA signals for space charge recovery in case of dielectric bilayer structures. The specificities to consider are among the following:

-calibration aspect owing to the fact that the influence charge evolves with time due to Maxwell interface polarisation;

-changes in sound velocity and impact on charge profile;

-reflection of acoustic waves at the interface due to acoustic impedance mismatch;

-acoustic response due to field step at the interface.

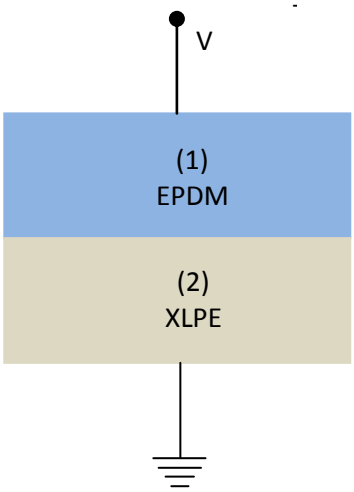

Figure 5: Bi-layer materials EPDM/XLPE

a) The calibration step

In the PEA method, the surface charge density used for calibration is first calculated by applying Gaussian theorem and boundary conditions on electric potential. It is assumed as a first approximation that the field distribution is capacitive and that the interface charge due to difference in conductivity between the two materials can be neglected during the calibration procedure. This assumption is verified a posteriori by considering the time constant necessary to establish interface charge compared to the polarization time of less than 1 min in calibration procedure. Under these conditions, the expression of capacitive charge located at the ground electrode in case of bilayers is given by:

$$\kappa_1 = \frac{\varepsilon_1 . \varepsilon_2 . U}{\varepsilon_1 . d_2 + \varepsilon_2 . d_1} \tag{16}$$

where ε_1, ε_2, d_1 and d_2 are respectively the permittivity and the thicknesses of insulating layers 1 and 2. U is the applied voltage.

b) The acoustic impedance match

Acoustic waves can be reflected at the interface between the two materials due to acoustic impedance mismatch. In the facts, acoustic reflections are more often accounted for at the interface with the electrodes where the mismatch is larger rather than between dielectrics [18]. This is supported by the fact that the acoustic impedance of polymers does not vary substantially from one material to another [19]. For this reason, semi-conductive layers with acoustic impedance similar that of a tested insulation are used as top electrode in the PEA cell. In detail, the transmission coefficient from material 1 to material 2 obtained from conservation of stress is defined as [8]:

$$T_{12} = \frac{2 \times Za_2}{Za_1 + Za_2} \tag{17}$$

where Za is the specific acoustic impedance defined as the product between sound velocity and specific density. With data given in Table 1, T_{12} exceeds 99% which means that the matching is excellent in this case. Note that depending on the relative values of impedance, the amplitude of the waves can be decreased or increased when crossing the interface.

Table 1. Dielectric and acoustic properties of tested materials (for density, standard values given)

Material	Relative permittivity ε_r	Sound velocity (m/s)	Density	Acoustic impedance Za (kg/m²/s)
EPDM	2.9	1800	1.10	1980
XLPE	2.3	2100	0.93	1950

c) The velocity difference for charge recovery

According to the expression (16), the space charge distribution at the origin of raw signals $v_{PEA}(t)$ is given by:

$$\rho(t(x)) = \frac{1}{v_s(x)} \mathrm{Re}\left[F^{-1}\left\{\frac{V_{PEA}(f)}{H_{setup}(f)}\right\}\right] \quad (18)$$

where

$$h_{setup}(t) = \frac{1}{\kappa_1} v_{PEA1}(t) \quad (19)$$

$V_{PEA}(f)$ and $H_{setup}(f)$ are respectively calculated by the Fourier transform of temporal signals $v_{PEA}(t)$ and $h_{setup}(t)$. $v_s(x)$ is the velocity profile of sound in bilayer sample (v_{s1} and v_{s2} in materials 1 and 2 respectively). Position x and time t are linked by the relationship: $x = v_s(x)*t$. As shown in Figure 6, a simple homothetic variation on time (t) of profile $\rho(t)$, obtained by deconvolution of PEA raw signals, makes it possible to obtain the space charge profile as a function of position $\rho(x)$ [20].

d) Response due to permittivity gradient

Holé et al. [21] used the general expression for the force density in a dielectric under field with 4 contributions related to the variation of the dielectric constant, to the effect of electrostriction, and to the presence of charges and of permanent dipole densities in an electric field. Whereas in a homogeneous material the contributions can be greatly simplified, it is not the case with stacked dielectrics and more generally inhomogeneous materials. In 1D and supposing that there is no permanent polarization (as could be with ferroelectrics), the force density (per unit volume) is expressed as:

$$f_s = -\frac{1}{2}E^2\frac{\partial \epsilon}{\partial x} - \frac{1}{2}\frac{\partial(\alpha E^2)}{\partial x} + \rho E \tag{20}$$

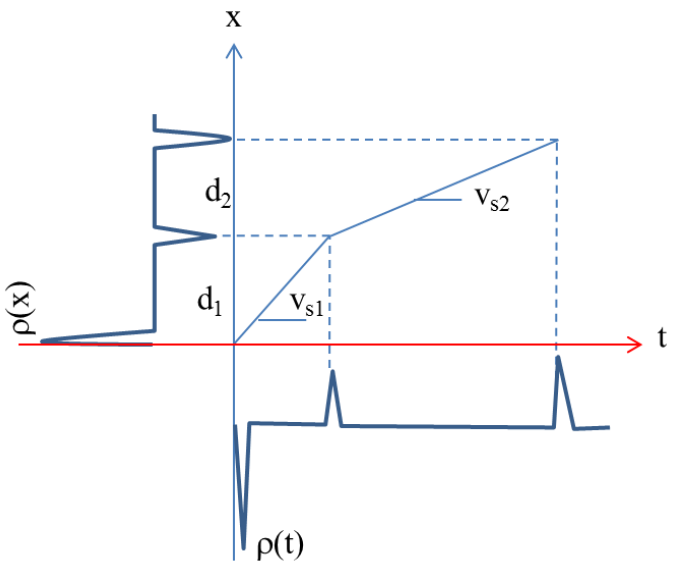

Figure 6: Determination of space charge profile versus position from space charge profile versus time from deconvolution of PEA raw signals in dielectric bilayers.

Under a pulse field δE_p, neglecting second order terms, the transient force can be expressed as:

$$\delta f_s = -E_{DC}\frac{\partial(\epsilon + \alpha)}{\partial x}\delta E_p - \alpha\frac{\partial E_{DC}}{\partial x}\delta E_p + \rho\delta E_p \tag{21}$$

where α is the electrostriction coefficient and E_{DC} represents the static field. The Equation (21) shows that in presence of a field gradient, a transient force is generated (second term) due to the electrostriction effect. The permittivity gradient existing at the interface between two dielectrics also leads to a transient pressure. Under applied DC stress, the pressure, obtained by integration along the x-direction defined by Figure 1, is of the form [22]:

$$\delta p_s = -D\left(1 - \frac{\epsilon_2}{\epsilon_1}\right)\delta E_p \tag{22}$$

where D is the electric displacement (homogeneous across the interface in absence of interface charges). So the pressure generated at the interface should appear as a fraction of the capacitive charge.

Bodega et al. [22] concluded on the fact that generally, when a multi-dielectric is tested, the detected acoustic signal does not correspond to the space charge distribution. The reasons are on the one hand the presence of an acoustic response with distributed permittivity, even in the absence of interfacial charge, cf. Eq. 22. The other aspect is linked to the fact that the detected acoustic signal does not correspond to the pressure distribution if the layers of the multi-dielectric have different

acoustic properties. A second consequence of acoustic mismatching is overlapping of reflected waves with the waves representing the pressure distribution inside the multi-dielectric.

C. Example of results for stacked dielectrics

Let us consider now an example of results obtained with the XLPE/EPDM structure. Figure 7 shows a mapping of space charge profiles in material XLPE (a) and bilayer XLPE/EPDM (b) at 40^0C under various applied electric fields obtained by deconvolution of raw PEA signals. The specific procedures adopted here to treat the rough data concern the accurate estimation of the interface charge in the calibration step (Eq. 15) and the correction for the sound velocity gradient. In case of multi-layer dielectric, much more charges are detected, one of the reasons being the presence of the interface. The analysis of the charge build and charge decay, considering amount, sign, and kinetic is proposed elsewhere [20, 23]. A pretty good agreement was obtained between results obtained by conductivity measurements and space charge build-up, i.e. independent experiments, and modelling with accounting for Maxwell-Wagner interface charge process.

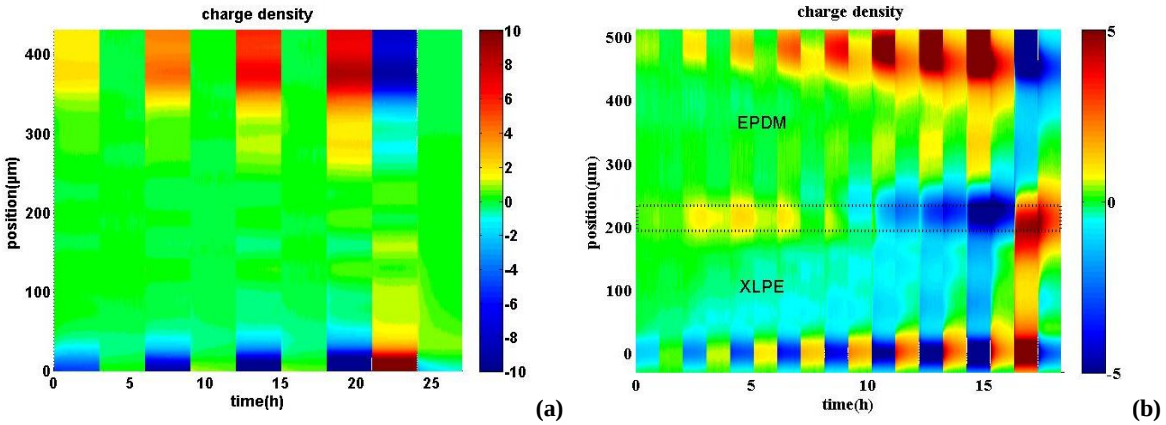

Figure 7: Mapping of space charge profiles in XLPE material (a) and bilayer XLPE/EPDM (b) at 40°C under different applied electric field. The color bar represents the scale for charge density in C/m^3. In a): applied fields were 10, 20, 30 and 40kV/mm followed by polarity reversal. In b): average fields were from 2 to 30kV/mm [20].

Regarding specific acoustic phenomena linked to the multilayer nature, the fact that the acoustic impedance of the two materials is the same avoids having spurious reflections. The permittivity on its own side is different from one material to the other, see Table 1. However, even though there is such contrast, we did not observe in an evident way a specific signal due the permittivity gradient. In absence of interface charge, the acoustic signal due to permittivity gradient should produce an apparent charge of the same sign as the capacitive charge on the higher permittivity material [22] i.e. EPDM. This was not observed in the present results. The detected signal is fully consistent with Maxwell-Wagner interface polarization and even the change in sign of the interface with increasing field could be explained by the behaviour of nonlinear conductivity in the two materials. There can be

two reasons for the absence of acoustic response: i/ it can be quickly overlapped by the interface polarization, or the permittivity values given here for a frequency of 50Hz are not the same at the DC limit or a frequency of the voltage pulses.

4. PEA method for model cable

A. PEA-cable device

The first PEA system for space charge measurement in a cable appeared in the 1990s [24], [25], [26]. The initial device was equipped with a curved electrode system (fixed radius of curvature) and was therefore adapted to a single type of cable. Difficulties arise naturally when one wants to make measurements on cables with different radius. To overcome this limitation, a flat-electrode PEA system now replaces the original device [27] and the PEA method is considered one of the most efficient techniques for measuring space charge in high voltage model cables [28]. An example of PEA cable mounting developed by TechImp, Italy, is shown in Figure 8.

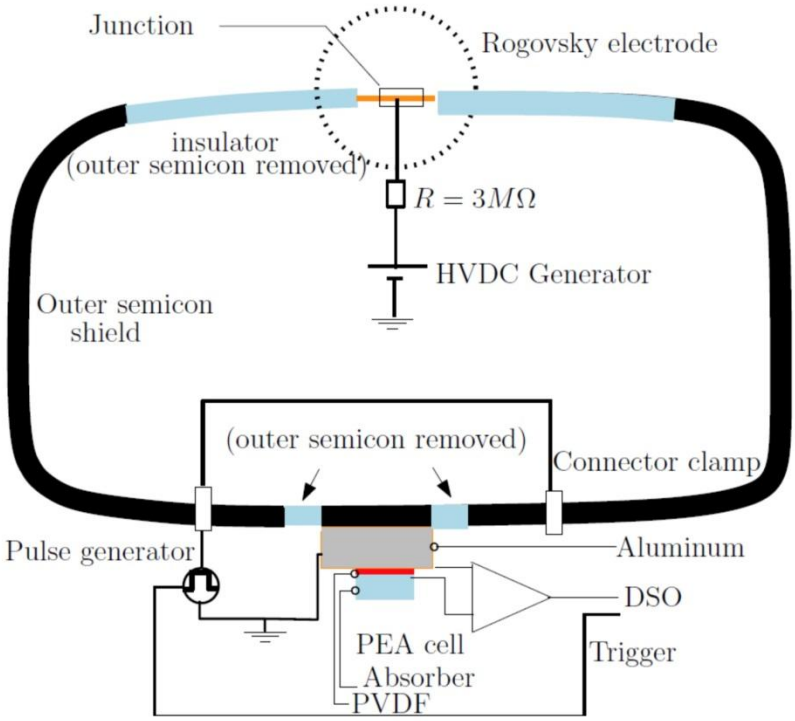

Figure 8: Sketch of PEA cable test rig [9]

The cable is attached to the PEA sensor cell by mounting bracket to adjust cable clamping, thus ensuring good acoustic contact between outer semiconductor of the cable and aluminium electrode of measurement cell. The pulsed voltage is injected at the measurement zone via outer semiconductor of cable by a pulse generator of 5kV maximum amplitude, 30ns width and 10 kHz of repetition rate. The outer semiconductor is removed over a 5 cm length between the measurement point and the region where pulses are applied. In this way, the cable itself is used as a decoupling capacitor. To ensure that

pulsed voltage at measuring point is high enough, the length of outer SC at point of application of the pulse is kept larger compared to that at the measuring point. A 100 kV high-voltage generator supplies the DC voltage, which is applied at conductor via a Rogovsky electrode. This type of electrode is used to avoid any field intensification.

For measurements at different temperatures, the cable is heated by an alternating current flowing in the cable core with control through a current transformer. In this way, a thermal gradient appears within the insulation since the cable surface is in contact with ambient air. The temperature at the surface of the cable is measured using a thermocouple. The current flowing in the cable is measured using an ammeter clamp. Knowledge of these two quantities and of the cable geometry enables to estimate cable core temperature.

B. Deconvolution in coaxial geometry

Recall that PEA method relies on detection of electrostatic forces generated by the interaction between internal charges and external electric pulse [29]. The propagation of acoustic waves towards the piezoelectric sensor is affected mainly by attenuation and dispersion. These phenomena are even more important when the insulating layer is relatively thick, for example in case of medium voltage cable samples (MV cable). In addition, the generation and propagation of acoustic waves are affected by the geometry of the cable [30]. Due to the divergence of electric field in coaxial geometry, the contribution to PEA signals of electrostriction force resulting from variation of permittivity induced by mechanical deformation of the polymer, during acoustic wave generation must be taken into account [21]. Following the same development as above for flat specimen, for a homogeneous material, in cylindrical geometry, the transient force density generated by the interaction of the static DC field and the electric pulse field at the radius r can be expressed as follows [31]:

$$\delta f_s(r) = \frac{\varepsilon}{r}.\frac{d}{dr}(rE_{DC}(r)).\delta E_p(r) - \alpha.r.\frac{d}{dr}\left(\frac{E_{DC}(r)}{r}\right)\delta E_p(r) \qquad (23)$$

The first term represents the response due to the space-charge induced field distortion (without space charge, the divergence of the field is null) and the second one is the electrostriction contribution, stating that the strain due to the non-homogeneity of electrical stress induces a variation on the relative permittivity which generates an elastic force.

Hence, the deconvolution method used for cable requires correction of attenuation, dispersion, and electrostriction as well as the PEA instrument response (sensor + voltage pulse) for recovering space charge profiles from PEA raw signals. The flowchart of deconvolution technique used for PEA-cable rough data is presented in Figure 9. The different steps are detailed in the following.

The deconvolution requires an accurate description of the whole system which is composed by the measuring instrument and the tested cable. The calibration procedure is used to establish the transfer function of the system. This step consists of acquiring raw signal from capacitive charges generated by application of DC voltage (U_{cal}). The PEA signal detected at the piezoelectric sensor $v_{PEA}(t)$ is given by the following expression [31]:

$$v_{PEA}(t)=h_{setup}(t)*[m_{rE}.g(r_E,t)+m_{rI}.g(r_I,t)] \quad (24)$$

where r_I and r_E are the inner and outer radius of cable. $h_{setup}(t)$ and $g(r,t)$ are respectively the transfer function of instrument and cable through which is taken into account the propagation of acoustic waves in the polymer material. m(r) is an intermediate variable depending on the cable radius (r) and the applied electric field $E_{DC}(r)$ [31]. Notably, it contains the term related to electrostriction.

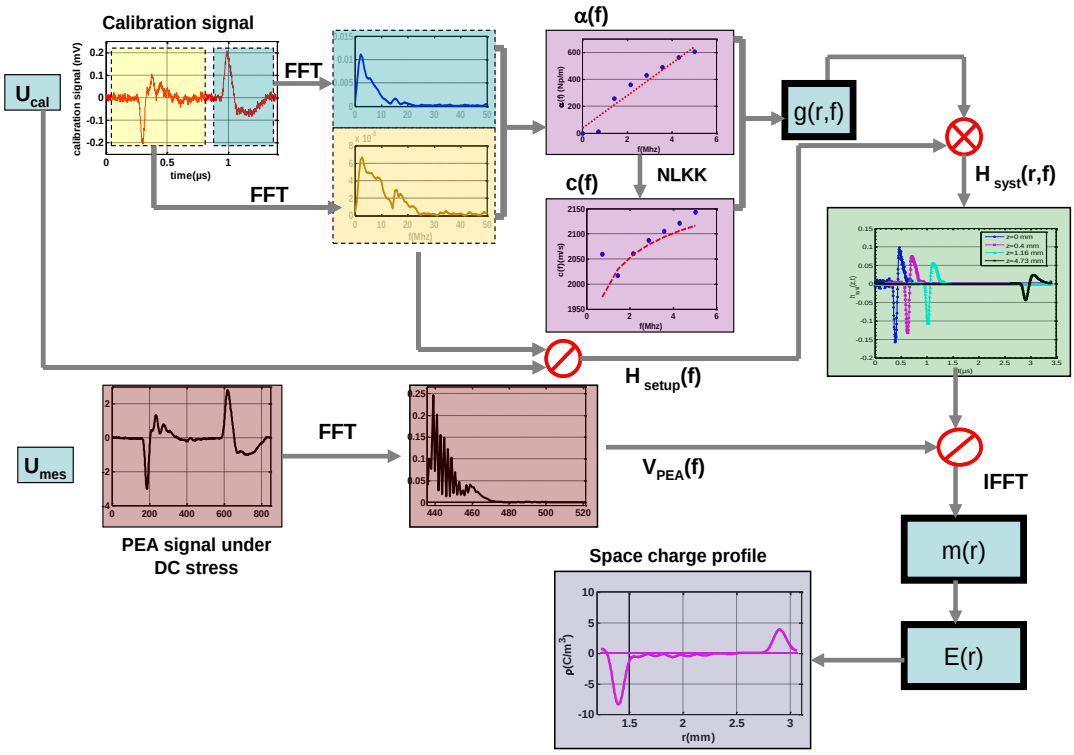

Figure 9: Synoptic of deconvolution method on PEA cable

The PEA calibration signal consists of two parts due to the responses of capacitive charges at the external $v_{PEA1}(t)$ and internal electrodes $v_{PEA2}(t)$ (Fig. 9). $g(r_E,t)$ is the Dirac function of time at the position r_E. Consequently, the first part of PEA signal, $v_{PEA1}(t)$, makes it possible to derive the instrument transfer function $h_{setup}(t)$ [31]:

$$h_{setup}(t) = \left(\frac{1}{m_{rE}}\right).v_{PEA1}(t) \quad (25)$$

The second part of PEA calibration signal in Equation (24) is generated by the capacitive charges located at the internal electrode (cable core) and therefore contains information related to the acoustic wave propagation (in particular attenuation coefficient and phase velocity). In the frequency domain, $V_{PEA2}(f)$ is given by the expression below:

$$V_{PEA2}(f) = H_{setup}(f).m_{rI}.G(r_I, f) \tag{26}$$

where $H_{setup}(f)$ and $G(r,f)$ are the Fourier transform of $h_{setup}(t)$ and $g(r,t)$. $G(r,f)$ is the transfer function of the cable through which is taken into account attenuation effects $\alpha(f)$ and dispersion $c(f)$ of the acoustic waves in the cable. The frequency spectra of attenuation coefficient and phase velocity can be deduced from the spectrum of the two parts of calibration signal. This procedure for determination of ultrasonic attenuation and phase velocity in solid dielectrics was initially introduced by Ditchi et al. [32]:

$$\alpha(f) = \frac{-1}{d}\log\left|\frac{V_{PEA2}(f)}{V_{PEA1}(f)}\left(\frac{r_I}{r_E}\right)^{3/2}\right| \tag{27}$$

$$c(f) = \frac{2\pi f d}{\varphi(V_{PEA1}(f)) - \varphi(V_{PEA2}(f))} \tag{28}$$

where $d = r_E - r_I$ and φ is the phase of the spectrum of the PEA signal.

The global transfer function $H_{syst}(f)$ of the system is obtained by multiplying the transfer function of the cable $G(r,f)$ and that of the instrument $H_{setup}(r, f)$. Thus, any PEA signal can be modelled in the frequency domain by equation 29:

$$V_{PEA}(f) = \sum_{j=1}^{N} H_{syst}(r_j, f).m(r_j) \tag{29}$$

The intermediate function $m(r)$ is calculated by the inverse Fourier transform of the ratio between the signal $V_{PEA}(f)$ and the transfer function of the system $H_{syst}(f)$. The electric field profile $E(r)$ and the space charge density profile $\rho(r)$ are derived from $m(r)$.

C. Example of results for MV cable

Figure 10 presents a map of space charge density (a) and of electric field profiles (b) obtained at different times on a MV cable with -40kV applied for 3h to the cable conductor. Then the voltage was removed for 30min before increasing the voltage to -80kV. In Fig.10b, after 200 s at -40 kV, since the material is free of charge, the field distribution is similar to the Laplacian field (for which the field value is -12.5 kV/mm at the inner electrode and -6.5 kV/mm at the outer electrode). Then, due to the negative homocharges build-up (see Figure 10a, blue zone at cathode) the field decreases at the

cathode and practically vanishes after 3 hours of polarization and increases in the bulk reaching a maximum value of about 12.5 kV/mm at r=8 mm.

Due to the presence of negative charges at the beginning of polarization under -80 kV, the electric field shape is similar to that at the end of polarization step under -40 kV and the maximum enhancement is found at 8 mm. At the end of the second polarization step, the maximum electric stress is located at the outer electrode due to heterocharge build-up. The field at the outer radius is estimated to about 22 kV/mm, which corresponds to the value of the geometrical field at the inner electrode for an applied voltage of -80 kV.

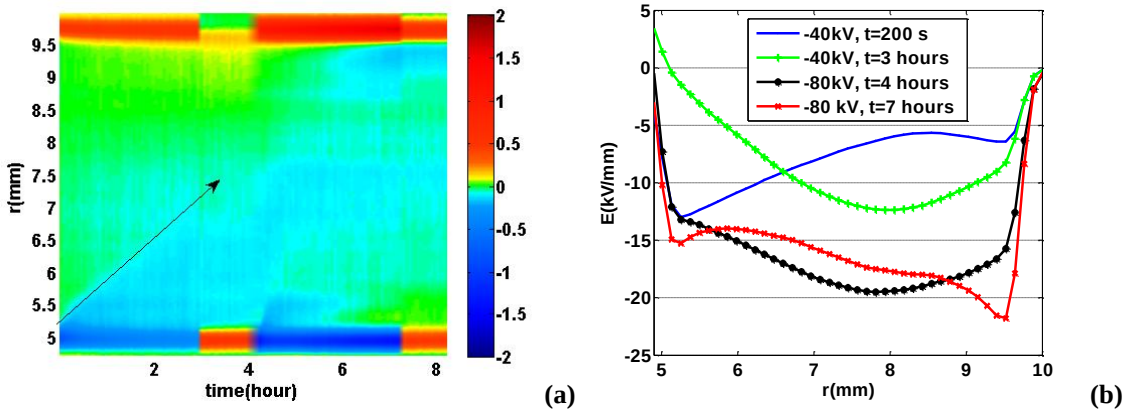

Figure 10: Map of space charge density (a) and electric field distribution profiles (b) in a medium voltage cable stressed under -40 kV and -80 kV at room temperature and different times.
The colour bar represents the scale for charge density in C/m^3.

D. Impact of acoustic properties of materials

From calibration taken on XLPE-insulated MV cables, the frequency dependence of acoustic properties given in Figure 11 were obtained [31] using the Nearly Local Kramers-Kronig (NLKK) approximation. Using a pulse width of typically 30ns, a sensor of 25µm thickness, and outer semicon thickness of 500µm (which can contribute to broaden the response), the acoustic response associated with the calibration signal is typically in the frequency range from 1 to 10 MHz for a MV cable.

Figure 11 shows that the higher the frequency the stronger the attenuation. For insulation thickness of 4.5mm the attenuation factor is typically of 20% at 1MHz and over 93% at 9MHz. Because of this feature, the pulse shape must be adapted to the thickness of sample to be probed, as a compromise between spatial resolution and damping of the acoustic signal. The linear variation of the attenuation coefficient vs. frequency is consistent with literature reports on acoustic properties of various polymers [33] [34], though from a mathematical point of view, it brings some inconsistency in the application of the Kramers-Kroning relations and the relation of attenuation and dispersion [35]. The value of α of about 600m^{-1} at 10MHz appearing in Figure 10 is in full agreement with those reported

earlier for polyethylene ([33], [34]). This linear dependence, called hysteresis absorption, has been explained by the freezing of the polymer in one of its many local energy minima [33]. Relaxation processes bring contributions in the form of deviation from the linear dependence [33], [34], especially at high frequencies (>10MHz). This means that the absorption depends on the free volume, and for crystalline polymers, on the degree of crystallinity. The attenuation changes substantially from one material to another, examples being $\alpha \approx 150 m^{-1}$ at 10MHz for PMMA (amorphous) and $\approx 800 m^{-1}$ PEO with 80% crystallinity. The absorption increases with the crystalline fraction and a second effect for crystalline polymers is the scattering of waves by crystalline regions as observed for high crystalline materials like poly(tetrafluoroethylene) for example. Hartman and Jarzynski [33] proposed an expression of following the form for the volume and velocity dependence of the absorption, which also accounts for the temperature variation:

$$\alpha(T,f) = \frac{a - bV(T)}{v(T)/f} \tag{30}$$

where a and b are constant for a given polymer. V is the volume of the polymer and *v* the sound velocity. The above considerations on materials acoustic properties have two consequences in practical implementation of the PEA method.

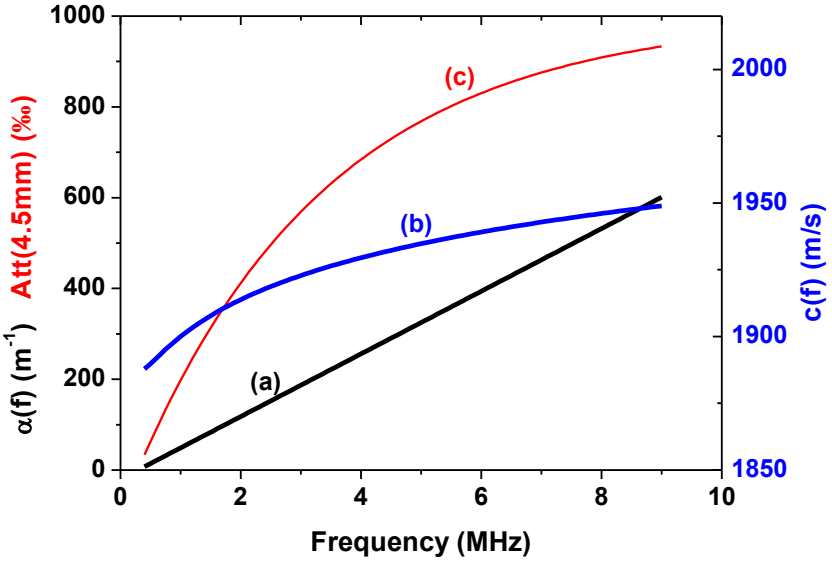

Figure 11: Frequency dependence of the attenuation coefficient (a) and sound velocity (b) from XLPE obtained from PEA calibration on a MV cable.
Line (c) represents the attenuation of acoustic wave across a 4.5mm thick insulation.

First, the temperature dependence of acoustic properties should be analysed when measurements are achieved under temperature gradient. In a temperature span of 20°C, according to literature data on PE [34], the velocity decreases by about 10%. So a correction similar to that achieved for bilayers

should be achieved in the time to position transformation. The temperature dependence of the attenuation does not vary in a monotonous way vs. temperature: the variation is primarily dependent on the thermal expansion coefficient variations and on relaxation features in the investigated temperature range [34]. Xia et al. [36] amended the system transfer function by adding quadratic approximation to the dispersion coefficients for calibration in coaxial geometry under temperature gradient.

Second, from the attenuation of acoustic waves, one can immediately anticipate the limitation in spatial resolution linked to materials behavior. With increasing the frequency (i.e. using shorter voltage pulses to improve the resolution), the attenuation increases substantially, meaning that measurements under higher resolution must go with thinner samples. By doing so, resolution of 1 to 2 μm could be reached on thin sample (50 μm) provided sensor thickness and pulse waveform were modified accordingly [37, 38].

5. Conclusion

In this work, the principle of deconvolution techniques for the PEA method in case of three different kinds of sample (flat, bilayer materials and geometric cables) has been described. PEA signal from the calibration procedure is used to build the system transfer function by deriving the frequency-dependent attenuation coefficient and the phase velocity. Application of these deconvolution techniques enables to observe space charge and stress distribution after few hours of polarization in material with different geometry and further to study mechanisms at the origin of charge build-up in such samples. The deformation of acoustic waves when travelling across the material can be relatively well accounted for, along with the dependence of their magnitude upon the perturbation pulse field in case of divergent geometry. However, the acoustic signal produced by indirect effects of charges, such as the electrostrictive forces due to non-homogeneous electric field is not easy to recover and to discriminate from the total signal since the actual field distribution should be known.

6. Acknowledgment

We are grateful to B Vissouvanadin for his advises and provision of figures for the manuscript.

7. References

[1] T. Mizutani, “Space charge measurement techniques and space charge in polyethylene,” IEEE Trans. Dielectr. Electr. Insul., vol. 1, pp. 923–933, 1994.

[2] S. Holé, T. Ditchi, and A. Lewiner, “Non-destructive methods for space charge distribution measurements: what are the differences?”, IEEE Trans. Dielectr. Electr. Insul., vol. 10, pp. 670–677, 2003.

[3] P. Notingher, S. Holé, L. Berquez, and G. Teyssedre, "An insight into space charge measurements", Internat. J. Plasma Environmental Sci. Technol., vol. 11, pp. 26-37, 2017.

[4] T. Takada and T. Sakai, “Measurement of electric fields at a dielectric/electrode interface using an acoustic transducer technique,” IEEE Trans. Electr. Insul., vol. 18, pp. 619–628, 1983.

[5] T. Maeno, T. Futami, H. Kushibe, T. Takada, and C.M. Cooke, “Measurement of spatial charge distribution in thick dielectrics using the pulsed electroacoustic method,” IEEE Trans. Electr. Insul., vol. 23, pp. 433–439, 1988.

[6] N. Hozumi, H. Suzuki, T. Okamoto, K. Watanabe, and A. Watanabe, “Direct observation of time-dependent space charge profiles in XLPE cable under high electric fields", IEEE Trans. Dielectr. Electr. Insul., vol. 1, pp. 1068–1076, 1994.

[7] H. Kitajima, Y. Tanaka, and T. Takada, "Measurement of space charge distribution at high temperature using the pulsed electro-acoustic (PEA) method," Proc. 7th Int'l. Conf. Dielectr. Materials, Meas. Appl., Bath, UK, pp. 8-11, 1996.

[8] J.B. Bernstein, “Analysis of the electrically stimulated acoustic-wave method for observing space charge in semi-insulating films”, Phys. Rev. B, vol. 44, pp. 10804-10814, 1991.

[9] B. Vissouvanadin, “Matériaux de câble à isolation synthétique pour des applications au transport d’énergie HVDC,” Thèse, Université Paul-Sabatier, Toulouse, 2011.

[10] C Thomas, G Teyssedre, and C. Laurent, "Space charge dynamic in polyethylene: from DC to AC stress", J. Phys. D: Appl. Phys., vol. 44,pp. 015401-01/08, 2011.

[11] T. Takada, O. Kisanuki, M. Sakata, and M. Uchiumi, "Characteristics of space charge formed in a laminated LDPE/EVA dielectric under DC stress", Proc. IEEE Int'l. Sympos. Electr. Insul., pp. 184‑187, 1996.

[12] S.T. Li, N. Zhao, Y.J. Nie, X. Wang, G. Chen, and G. Teyssedre, "Space charge characteristics of LDPE nanocomposite/LDPE insulation system", IEEE Trans. Dielectr. Electr. Insul., vol. 22, pp. 92-100, 2015.

[13] Z. Xu and G. Chen, "Interfacial characteristics of space charge in multi-layer LDPE", Proc. 2008 Internat. Conf. Condition Monitoring and Diagnosis, Beijing, China, pp. 1-4, 2008.

[14] I. Iddrissu, S. M. Rowland, and A. Tzimas, "The Impact of interfaces and space charge formation on breakdown strength of epoxy resin", Proc. IEEE Conf. Electr. Insul. Dielectr. Phenomena (CEIDP), pp. 90-93, 2014.

[15] P. H. F. Morshuis, R. Bodega, D. Fabiani, G. C. Montanari, L. A. Dissado, and J. J. Smit, "Dielectric interfaces in DC constructions: Space charge and polarization phenomena", Proc. IEEE Int'l. Conf. Solid Dielectr. (ICSD), pp. 450-453, 2007.

[16] M. Huang, Y. Zhou, Q. Sun, Y. Sha, and L. Zhang, "Effect of interface on space charge behavior in Multi-layer Oil-Paper insulation", Proc. IEEE Conf. Electr. Insul. Dielectr. Phenomena (CEIDP), pp. 654‑657, 2012.

[17] J. Beyer, P.H.F. Morshuis, and J.J. Smit, "Space charge phenomena in laminated HVDC insulation", Proc. 1998 Internat. Symp. Electr. Insul. Materials (ISEIM), Toyohashi, Japan, pp. 181-186, 1998.

[18] G. Mier-Escurra, A. Rodrigo-Mor, and P. Vaessen, "A calibration method for acoustic space charge measurements using multilayer samples", Sensors, vol. 18, pp. 2508-2518, 2018.

[19] T. Maeno, "Calibration of the pulsed electroacoustic method for measuring space charge density", IEEJ Transactions on Fundamentals and Materials, vol. 119, pp. 1114-1119, 1999.

[20] T.T.N. Vu, G. Teyssedre, B. Vissouvanadin, S. Le Roy, and C. Laurent, "Correlating conductivity and space charge measurements in multi-dielectrics under various electrical and thermal stresses", IEEE Trans. Dielectr. Electr. Insul., vol. 22, pp. 117-127, 2015.

[21] S. Holé, “Influence of divergent electric fields on space-charge distribution measurements by elastic methods,” Phys. Rev. B, vol. 61, pp. 13528–13539, 2000.

[22] R. Bodega, P. H. F. Morshuis, and J. J Smit, “Space charge measurements on multidielectrics by means of the pulsed electroacoustic method”, IEEE Trans. Dielectr. Electr. Insul., Vol. 13, pp. 272-281, 2006.

[23] T.T.N. Vu, G. Teyssedre, S. Le Roy, and C. Laurent, "Maxwell-Wagner effect in multi-layered dielectrics: interfacial charge measurement and modelling", Technologies, vol. 5, 27, 2017.

[24] M. Yasuda, M. Ito, and T. Takada, “Measurement of charge distributions in coaxial cable using the pulsed electroacoustic method,” Jpn. J. Appl. Phys., vol. 30, pp. 71–73, 1991.

[25] N. Hozumi, T. Okamoto, and T. Imajo, “Space charge distribution measurement in a long size XLPE cable using the pulsed electroacoustic method,” Conf. Rec. 1992 IEEE Int. Symp. Electr. Insul., pp. 294 – 297, 1992.

[26] R. Liu, T. Takada, and N. Takasu, “Pulsed electro-acoustic method for measurement of space charge distribution in power cables under both DC and AC electric fields,” J. Phys. D, vol. 26, pp. 986–994, 1993.

[27] M. Fu, G. Chen, A.E. Davies, and J.G. Head, “Space charge measurement in power cables using a modified PEA system,” Proc. 8th Int. Conf. Dielectr. Mater. Meas. Appl., pp. 74-79, 2000.

[28] T. Takada and N. Hozumi, “Space charge measurements as a diagnostic tool for power cables,” Proc. IEEE Power Eng. Soc. Winter Meet., pp. 1609–1614, 2000.

[29] T. Maeno, and K. Fukunaga, “High-resolution PEA charge distribution measurement system,” IEEE Trans. Dielectr. Electr. Insul., vol. 3, pp. 754–757, 1996.

[30] G. Chen, Y.L Chong, and M. Fu, “Calibration of the pulsed electroacoustic technique in the presence of trapped charge,” Meas. Sci. Technol., vol. 17, pp. 1974–1980, 2006.

[31] B. Vissouvanadin, T.T.N. Vu, L. Berquez, S. Le Roy, G. Teyssedre, and C. Laurent, “Deconvolution techniques for space charge recovery using pulsed electroacoustic method in coaxial geometry,” IEEE Trans. Dielectr. Electr. Insul., vol. 21, pp. 821–828, 2014.

[32] T. Ditchi, C. Alquié, and J. Lewiner, “Broadband determination of ultrasonic attenuation and phase velocity in insulating materials,” J. Acoust. Soc. Am, vol. 94, pp. 3061–3065, 1993.

[33] B. Hartmann and J. Jarzynski, "Ultrasonic hysteresis absorption in polymers", J. Appl. Phys., vol. 43,pp. 4304-4312, 1972.

[34] K. Adachi, G. Harrison, J. Lamb, A. M. North, and R. A. Pethrick, "High frequency ultrasonic studies of polyethylene", Polymer, vol. 22, pp. 1032-1039, 1981.

[35] K. R. Waters, J. Mobley, and J. G. Miller, "Causality-imposed (Kramers-Kronig) relationships between attenuation and dispersion", IEEE Trans. Ultrason., Ferroelect., Freq. Contr., vol. 52, pp. 822-833, 2005.

[36] X. Wang, C. Chen, J.Q. Hao, K. Wu, X. Chen, W.P. Li, and C. Zhang, "Recovery Algorithm for Space Charge Waveform in Coaxial Cable under Temperature Gradient", Sensors and Materials, vol. 29, pp. 1147–1157, 2017.

[37] L. Galloy, L. Berquez, F. Baudoin, and D. Payan, "High-resolution pulsed electro-acoustic (HR PEA) measurement of space charge in outer space dielectric materials", IEEE Trans. Dielectr. Electr. Insul., Vol. 23, pp. 3151-3155, 2016.

[38] K. Kumaoka, T. Kato, H. Miyake, and Y. Tanaka, "Development of space charge measurement system with high positional resolution using pulsed electro acoustic method," Proceedings of 2014 International Symposium on Electrical Insulating Materials, Niigata, pp. 389-392, 2014.

Thi Thu Nga Vu was born in 1981 in Hanoi, Vietnam. She received the Master's degree in 2007 from the Hanoi University of Science and Technology, in Vietnam. She received the Ph.D. degree in electrical engineering from the University of Toulouse, France, in 2014 for a research work on space phenomena in polymeric insulating materials intended for HVDC cable application at the Laboratory of Plasma and Energy Conversion -Laplace in Toulouse, France. She has been working since 2004 as a researcher and lecturer at the Electric Power University in Hanoi, Vietnam.

Laurent Berquez was born in Abbeville, France, in 1970. He received the M.Sc. degree in acoustics in 1994, and the Ph.D. degree in 1998 from the Toulouse University. He is full professor at the Toulouse University and works on multi-dimensional mapping of polarization and space-charge distributions in thin dielectric polymers at the Laboratory of Plasma and Energy Conversion –Laplace in Toulouse. He is heading a research team working on the reliability of dielectrics in electrical equipment.

Gilbert Teyssedre was born in 1966 in Rodez, France. He received his Engineer degree in materials physics and Masters in solid state physics in 1989 at the National Institute for Applied Science (INSA). Then he joined the Solid State Physics Lab in Toulouse and obtained the Ph.D. degree in 1993 for work on ferroelectric polymers. He joined the CNRS in 1995 and has been working since then at the Laplace in Toulouse. His research activities concern luminescence techniques in insulating polymers with focus on chemical and physical structure, degradation phenomena, space charge and transport properties. He is currently Senior Researcher at CNRS in a team working on the reliability of dielectrics in electrical equipment.